Journal of Sound and Vibration (2002) **254**(2), 297–312
doi:10.1006/jsvi.2001.4088, available online at http://www.idealibrary.com on IDEAL®

THE UNBALANCED MAGNETIC PULL AND ITS EFFECTS ON VIBRATION IN A THREE-PHASE GENERATOR WITH ECCENTRIC ROTOR

D. Guo, F. Chu and D. Chen

Department of Precision Instruments, Tsinghua University, Beijing 100084, *People's Republic of China.*
E-mails: guod@pim.tsinghua.edu.cn; chufl@pim.tsinghua.edu.cn

(*Received* 23 *October* 2000, *and in final form* 13 *July* 2001)

The unbalanced magnetic pull (UMP) in a three-phase generator under no-load, caused by dynamic and static eccentricity, is calculated theoretically. The air-gap permeance is expressed as a Fourier series. Analytical expressions of the UMP for any pole-pair number are obtained. Effects of relative eccentricity and pole number on the magnitude of the UMP are obtained. The vibration of a model rotor in a three-phase generator under the action of the UMP and the eccentric force is analyzed by the numerical method and the harmonic analysis.

1. INTRODUCTION

Rotating electrical machines, which often have small air gaps, are especially vulnerable to slight variations in the dimensions of the stator, rotor, end rings and bearings, which can lead to significant variation of the air gap between the stator and the rotor at different angular positions. During operation, this non-uniform air-gap distorts the air-gap flux density distribution, which can produce appreciable unbalanced magnetic pull (UMP). The effect of UMP can be quite dangerous to the rotor.

There have been many methods for calculating UMP. Early papers such as Von Kaehne [1] and Binns and Dye [2] surveyed many empirically based formulae already available. In 1955, Summers [3] developed the theory of UMP by using rotating field components. Jordan [4–6] published much on the theoretical study about UMP with his co-researchers. These papers put forward the idea of modulating the fundamental MMF wave by the air-gap permeance expressed as a Fourier series. Smith and Dorrell [7] studied the UMP by winding analysis. Finite element analysis technique [8, 9] can now provide solutions of the UMP although this approach is still very computationally expensive and often cannot provide an insight into the origins and key factors in the production of UMP.

A literature survey indicates that there has been intensive study on the methods of calculating UMP. But, due to rotor eccentricity, there are several aspects of the UMP which still remain unclear. Few authors have tried to obtain the analytical expression of the UMP for any pole-pair machine, and only a few authors have studied the vibratory characteristics of the rotor system due to the UMP. They are Belmans *et al.* [10], Zhu *et al.* [11], and Fruchtenicht *et al.* [4]. Belmans *et al.* [10] studied the influence of the UMP on the radial stability of the shaft in a two-pole machine. They thought that owing to the UMP, an electromagnetically induced spring coefficient and damping coefficient were generated which resulted in the decrease of the natural frequency and the change of the total damping

0022-460X/02/$35.00

ratio. Zhu *et al.* [11] studied the effect of the rotor eccentricity on acoustic noise and vibration of the single-phase induction motors. Fruchtenicht *et al.* [4] investigated the self-excited transverse vibration of a four-pole machine due to the UMP.

Using the method based on the idea of modulating the fundamental MMF wave by the air-gap permeance expressed as a Fourier series, the analytical expression of the UMP produced in a three-phase electric machine with any pole-pairs and caused by static eccentricity and dynamic eccentricity, is obtained in this paper. Every component of the UMP is analyzed for different pole-pair number. The non-linear vibratory responses of a Jeffcott rotor excited by the UMP and eccentric force are studied by use of the numerical method—Newmark integral method. Several interesting center orbits are obtained. The frequency components of vibration are acquired and explained by harmonic analysis. The effects of the UMP on the vibration of the rotor system are concluded.

2. CALCULATION OF THE UMP

Figure 1 shows an eccentric rotor, and the air-gap length can be approximately expressed as

$$\delta(\alpha) \approx \delta_0 - r\cos(\alpha - \theta), \tag{1}$$

where δ_0 is the mean air-gap length when the rotor is centered.

From reference [12], the air-gap permeance can be expanded as a Fourier series

$$\Lambda(\alpha) = \frac{\mu_0}{\delta(\alpha)} = \frac{\mu_0}{\delta_0[1 - \varepsilon\cos(\alpha - \theta)]} = \frac{\mu_0}{\delta_0}\sum_{n=0}^{\infty}\varepsilon^n\cos^n(\alpha - \theta)$$

$$= \sum_{n=0}^{\infty}\Lambda_n\cos n(\alpha - \theta), \tag{2}$$

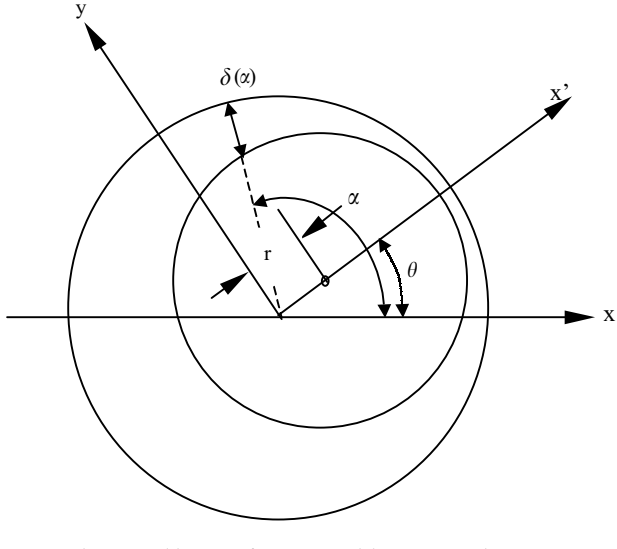

Figure 1. Air-gap of a motor with an eccentric rotor.

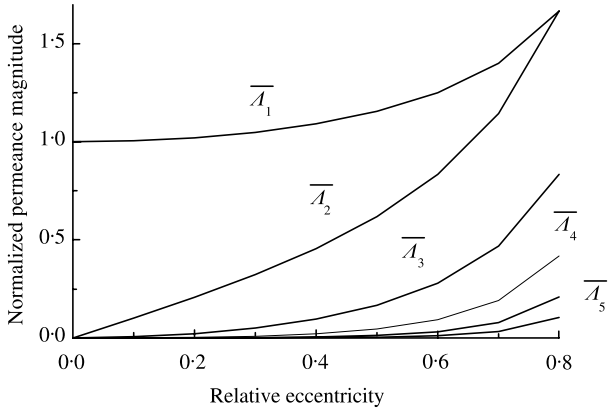

Figure 2. Air-gap permeance coefficient against eccentricity.

where ε is the relative eccentricity, and

$$\varepsilon = \frac{r}{\delta_0} \tag{3}$$

μ_0 is the air permeance. The Fourier coefficients Λ_n are

$$\Lambda_n = \begin{cases} \dfrac{\mu_0}{\delta_0} \dfrac{1}{\sqrt{1-\varepsilon^2}} & (n=0), \\ \dfrac{2\mu_0}{\delta_0} \dfrac{1}{\sqrt{1-\varepsilon^2}} \left(\dfrac{1-\sqrt{1-\varepsilon^2}}{\varepsilon} \right)^n & (n>0). \end{cases} \tag{4}$$

The normalized magnitudes of the permeance series can be represented by

$$\bar{\Lambda}_n = \frac{\Lambda_n \delta_0}{\mu_0} = \begin{cases} \dfrac{1}{\sqrt{1-\varepsilon^2}} & (n=0), \\ \dfrac{2}{\sqrt{1-\varepsilon^2}} \left(\dfrac{1-\sqrt{1-\varepsilon^2}}{\varepsilon} \right)^n & (n>0). \end{cases} \tag{5}$$

The relationship between $\bar{\Lambda}_n$ and the relative eccentricity ε is shown in Figure 2. From Figure 2, it can be seen that the first-harmonic component dominates. Hence, if the eccentricity is assumed to be small, only the first-harmonic component and the second-harmonic component need to be taken into account.

According to the theory of electric machine [13], the fundamental MMF of the air gap in a three-phase generator under no-load state can be expressed as

$$F(\alpha, t) = F_j \cos(\omega t - p\alpha), \tag{6}$$

where $\mathbf{F}_j$ is the amplitude of the fundamental MMF of the excitation current of the rotor. The air-gap flux density distribution is

$$B = \mu_0 \frac{F}{\delta} = \Lambda(\alpha, t) F(\alpha, t). \tag{7}$$

Substituting equations (4) and (6) into equation (7) and keeping the first four terms of the infinite series yield:

$$B = \frac{1}{2}F_j \sum_{n=0}^{\infty} \Lambda_n \{\cos[(p-n)\alpha - (\omega t - n\theta)] + \cos[(p+n)\alpha - (\omega t + n\theta)]\}$$

$$= \frac{1}{2}F_j \{2\Lambda_0 \cos(\omega t - p\alpha) + \Lambda_1 [\cos((p-1)\alpha - (\omega t - \theta)) + \cos((p+1)\alpha - (\omega t + \theta))]$$

$$+ \Lambda_2 [\cos((p-2)\alpha - (\omega t - 2\theta)) + \cos((p+2)\alpha - (\omega t + 2\theta))] + \Lambda_3 [\cos((p-3)\alpha$$

$$- (\omega t - 3\theta)) + \cos((p+3)\alpha - (\omega t + 3\theta))]\}. \tag{8}$$

From equation (8), it can be seen that the modulation of the harmonic MMF waves by air-gap permeance produces air-gap harmonic fields with different pole-pair numbers. It can also be observed from Figure 2 that the first-harmonic component dominates, then second harmonic. Because Λ_2 and Λ_3 are sufficiently small in comparison with Λ_0 and Λ_1 when the eccentricity is small, we need only to account for the MMF harmonic $\pm$ one pole-field harmonic. If the eccentricity is large, we need then the higher permeance harmonics.

The Maxwell stress normal to the iron/air boundary in terms of the flux density is [14]

$$\sigma = \frac{B^2}{2\mu_0}. \tag{9}$$

Substituting equation (8) into equation (9), we can obtain

$$\sigma = \sum_{i=0}^{6} \{a_i \cos i(\alpha - \theta) + b_i \cos[2\omega t - (2p-i)\alpha - i\theta] + c_i \cos[2\omega t - (2p+i)\alpha + i\theta]\} \tag{10}$$

where a_i, b_i and c_i are the functions of Λ_0, Λ_1, Λ_2, Λ_3, δ_0 and F_j. The calculation of a_i, b_i and c_i are quite lengthy. Therefore, it will not be shown here.

The resulting force can be obtained by integrating the horizontal and vertical components of the Maxwell stress over rotor surface as

$$P_x = \int_0^{2\pi} \sigma \cos\alpha \, RL \, \mathrm{d}\alpha, \tag{11}$$

$$P_y = \int_0^{2\pi} \sigma \sin\alpha \, RL \, \mathrm{d}\alpha. \tag{12}$$

Substituting equation (10) into equations (11) and (12), and assuming the eccentricity to be axially constant, we have

$$P_x^{UMP} = \begin{cases} f_1 \cos\theta + f_2 \cos(2\omega t - \theta) + f_3 \cos(2\omega t - 3\theta), & p = 1, \\ f_1 \cos\theta + f_3 \cos(2\omega t - 3\theta) + f_4 \cos(2\omega t - 5\theta), & p = 2, \\ f_1 \cos\theta + f_4 \cos(2\omega t - 5\theta), & p = 3, \\ f_1 \cos\theta, & p > 3 \end{cases} \tag{13a}$$

and

$$P_y^{UMP} = \begin{cases} f_1 \sin\theta + f_2 \sin(2\omega t - \theta) - f_3 \sin(2\omega t - 3\theta), & p = 1, \\ f_1 \sin\theta + f_3 \sin(2\omega t - 3\theta) - f_4 \sin(2\omega t - 5\theta), & p = 2, \\ f_1 \sin\theta + f_4 \sin(2\omega t - 5\theta), & p = 3, \\ f_1 \sin\theta, & p > 3, \end{cases} \tag{13b}$$

where

$$f_1 = \frac{RL\pi}{4\mu_0} F_j^2 (2\Lambda_0\Lambda_1 + \Lambda_1\Lambda_2 + \Lambda_2\Lambda_3), \tag{14a}$$

$$f_2 = \frac{RL\pi}{4\mu_0} F_j^2 \left(\Lambda_0\Lambda_1 + \frac{1}{2}\Lambda_1\Lambda_2 + \frac{1}{2}\Lambda_2\Lambda_3 \right), \tag{14b}$$

$$f_3 = \frac{RL\pi}{4\mu_0} F_j^2 \left(\Lambda_0\Lambda_3 + \frac{1}{2}\Lambda_1\Lambda_2 \right), \tag{14c}$$

$$f_4 = \frac{RL\pi}{8\mu_0} F_j^2 \Lambda_2\Lambda_3. \tag{14d}$$

Both force projections include two components. One is independent of time and represents the constant unbalanced magnetic pull with the magnitude of $\mathbf{f}_1$. Another component vibrates with its frequency equalling the double supply frequency and magnitude being the function of $\mathbf{f}_2$, $\mathbf{f}_3$ and $\mathbf{f}_4$. If the pole-pair number is larger than three, only the constant unbalanced magnetic pull remains. This is because the higher order harmonic forces counteract round the rotor surface when the pole-pair number is larger than three. In fact, we can find from Appendix A that the oscillating component of the UMP when $\mathbf{p} = 3$ is much less than that when $\mathbf{p} < 3$.

The normalized force magnitudes can be represented by

$$\bar{f}_n = \frac{4 f_n \delta_0^2}{RL\pi F_j^2 \mu_0} \, n = 1, 2, 3, 4. \tag{15}$$

The relationship between $\bar{f}_n$ and the relative eccentricity $\boldsymbol{\varepsilon}$ is shown in Figure 3. It can be seen from Figure 3 that the curves of $\mathbf{f}_1$, $\mathbf{f}_2$, $\mathbf{f}_3$ and $\mathbf{f}_4$ are all non-linear when the relative eccentricity is large. The $\mathbf{f}_1$ and $\mathbf{f}_2$ dominate if the eccentricity is small.

3. THE EFFECT OF UMP ON VIBRATION OF A GENERATOR ROTOR SYSTEM

A Jeffcott model is adopted in this paper. This model consists of a massless shaft with spring coefficient $\mathbf{k}$, damping coefficient c and a disk mass concentrated in the middle of the

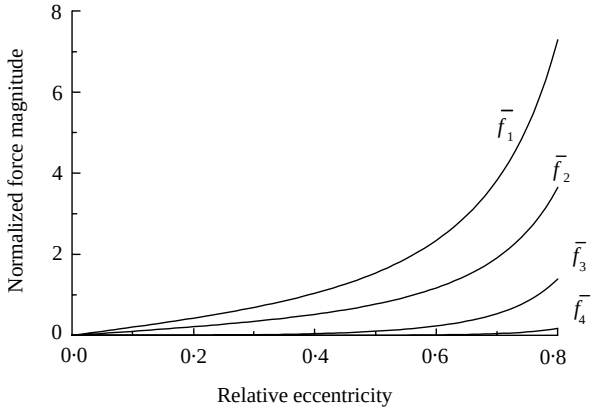

Figure 3. Force magnitude against eccentricity.

shaft having a value of **m**. The mass eccentric distance of the disk is *a*. The differential equations for the radial vibration of the rotor can be written as

$$\begin{aligned} m\ddot{x} + c\dot{x} + kx &= ma\Omega^2 \cos \Omega t + P_x^{UMP}(x, y, t), \\ m\ddot{y} + c\dot{y} + ky &= ma\Omega^2 \sin \Omega t + P_y^{UMP}(x, y, t), \end{aligned} \tag{16}$$

where $\boldsymbol{\Omega}$ is the rotating angular speed. The following parameters have been used

$$\begin{aligned} &c = 81{\cdot}9 \text{ Ns/m}, \quad k = 1{\cdot}526 \times 10^6 \text{ N/m}, \quad m = 18{\cdot}15 \text{ kg}, \\ &a = 0{\cdot}5 \text{ mm}, \quad R = 59 \text{ mm}, \quad L = 0{\cdot}1551 \text{ m}, \\ &\delta_0 = 2{\cdot}2 \text{ mm}, \quad F_j = 684 \text{ A}, \quad \omega = 50 \text{ Hz}. \end{aligned}$$

According to the theory of vibration, if the non-linear UMP is not taken into account, the natural frequency of the rotor system is

$$\omega_n = \frac{1}{2\pi} \sqrt{\frac{k}{m} - \left(\frac{c}{2m}\right)^2} = 46 \text{ Hz}. \tag{17}$$

From equations (A.1) and (A.2) of Appendix A, the amplitudes f_2, f_3, f_4 of the oscillating UMP are non-linear functions of the relative eccentricity ε, and $\varepsilon = \sqrt{x^2 + y^2}/\delta_0$. The UMP oscillates with a frequency of 2ω (two time power frequency). Therefore, equation (16) is a set of non-linear parametric vibration with forced vibration when $\mathbf{p} < 4$. Because the expression of the parametrically exciting force is complex, it is difficult to solve equation (16) by the analytical method. The implicit integration formula of the Newmark integral method [15] is then used to calculate the non-linear dynamic response of equation (16). Equation (16) at time $\mathbf{t}_{n+1}$ can be rewritten as

$$M\ddot{q}_{n+1} + C\dot{q}_{n+1} + Kq_{n+1} = P_{n+1}^e + P_{n+1}^{UMP}, \tag{18}$$

where

$$M = \begin{bmatrix} m & 0 \\ 0 & m \end{bmatrix}, \quad C = \begin{bmatrix} c & 0 \\ 0 & c \end{bmatrix}, \quad K = \begin{bmatrix} k & 0 \\ 0 & k \end{bmatrix}, \quad q_{n+1} = \begin{Bmatrix} x_{n+1} \\ y_{n+1} \end{Bmatrix}, \quad P^e_{n+1}$$

$$= \begin{Bmatrix} ma\Omega^2 \cos \omega t_{n+1} \\ ma\Omega^2 \sin \omega t_{n+1} \end{Bmatrix}, \quad P^{UMP}_{n+1} = \begin{Bmatrix} P^{UMP}_{x,n+1} \\ P^{UMP}_{y,n+1} \end{Bmatrix}$$

According to the implicit integration formula of the Newmark integral method, we have

$$q_{n+1} = \tilde{q}_{n+1} + \Delta t^2 \beta \ddot{q}_{n+1}, \qquad \dot{q}_{n+1} = \tilde{\dot{q}}_{n+1} + \Delta t^2 \gamma \ddot{q}_{n+1},$$

where

$$\tilde{q}_{n+1} = q_n + \Delta t \dot{q}_n + \Delta t^2 (1 - 2\beta) \ddot{q}_n / 2, \qquad \tilde{\dot{q}}_{n+1} = \dot{q}_n + \Delta t (1 - \gamma) \ddot{q}_n,$$

Δt is the time step, γ and β are the Newmark parameters, and we choose $\gamma = 0{\cdot}5$, $\beta = 0{\cdot}25$ in order to provide an unconditionally stable algorithm [15].

The iteration procedure of each time step is as follows:

(1) Set $i = 0$

$$q^{(i)}_{n+1} = \tilde{q}_{n+1} = q_n + \Delta t \dot{q}_n + \Delta t^2 (1 - 2\beta) \ddot{q}_n / 2,$$

$$\dot{q}^{(i)}_{n+1} = \tilde{\dot{q}}_{n+1} = \dot{q}_n + \Delta t (1 - \gamma) \ddot{q}_n,$$

$$\ddot{q}^{(i)}_{n+1} = [q^{(i)}_{n+1} - \tilde{q}_{n+1}] / (\Delta t^2 \beta).$$

(2) Calculate the residual force

$$\Psi^i_{n+1} = P^e_{n+1} + P^{UMP}(q^i_{n+1}) - M \ddot{q}^i_{n+1} - C \dot{q}^i_{n+1} - K q^i_{n+1}.$$

(3) Calculate the effective stiffness matrix

$$\tilde{K} = M / (\Delta t^2 \beta) + \gamma C_T / (\Delta t \beta) + K_T (q^i_{n+1}),$$

where K_T is the tangent stiffness matrix at q^i_{n+1}.

(4) Solve the following equation:

$$\tilde{K} \Delta q^i_{n+1} = \Psi^i_{n+1}.$$

(5) Revise displacement, velocity, acceleration and i

$$q^{i+1}_{n+1} = q^i_{n+1} + \Delta q^i_{n+1},$$

$$\ddot{q}^{i+1}_{n+1} = (q^{i+1}_{n+1} - \tilde{q}_{n+1}) / (\Delta t^2 \beta),$$

$$\dot{q}^{i+1}_{n+1} = \dot{q}_{n+1} + \Delta t \gamma \ddot{q}^{i+1}_{n+1},$$

$$i = i + 1$$

and then reduplicate the above process until $\|\Delta q_{n+1}^{(i)}\|/\|q_{n+1}^{(i+1)}\| \leqslant \lambda$, where λ is a known accuracy error.

The selection of the integral step length lies on the rotating speed of the rotor. The base on which the time step is chosen is the maximal oscillating frequency of the external force components. All initial conditions are assumed to be zero if not specially mentioned. The integration proceeds for quite a long time first to remove the effect of the initial conditions. Then the data are recorded for figures.

3.1. WHEN THE RELATIVE ECCENTRICITY IS SMALL

From Figure 3, we can see that the curves of $\mathbf{f}_1$, $\mathbf{f}_2$, $\mathbf{f}_3$ and $\mathbf{f}_4$ are almost linear when the relative eccentricity is small. We study the situation of $\mathbf{p} = 1$ first. The center of the rotor can be considered the same as the center of the stator at initial state. Non-homogenous air gap will exist when the rotor is whirling due to the mass eccentricity. This situation is usually called dynamic eccentricity. Figure 4(a) shows the orbits of the rotor center with UMP considered and not considered when $\mathbf{\Omega} = 5$ Hz. It can be seen that the vibration magnitude with UMP considered is larger than that with UMP not considered. From Appendix A, we know that the constant component of the UMP always pulls the rotor to the minimum air gap, and this makes the average orbit size of the rotor larger. The orbit with UMP existed is

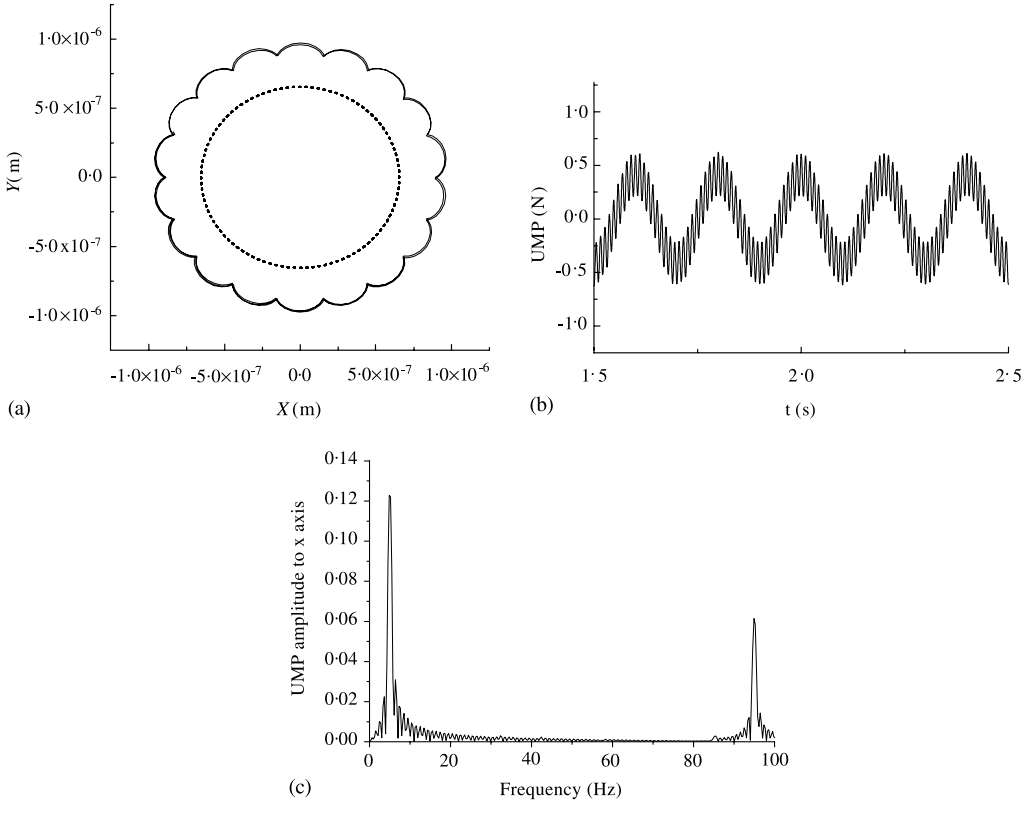

Figure 4. (a) Rotor center orbit when $p = 1$, $\Omega = 5$ Hz: ——, UMP existed; ·····, UMP not existed. (b) The curve of the UMP to time when $p = 1$, $\Omega = 5$ Hz. (c) The frequency components of the UMP when $p = 1$, $\Omega = 5$ Hz.

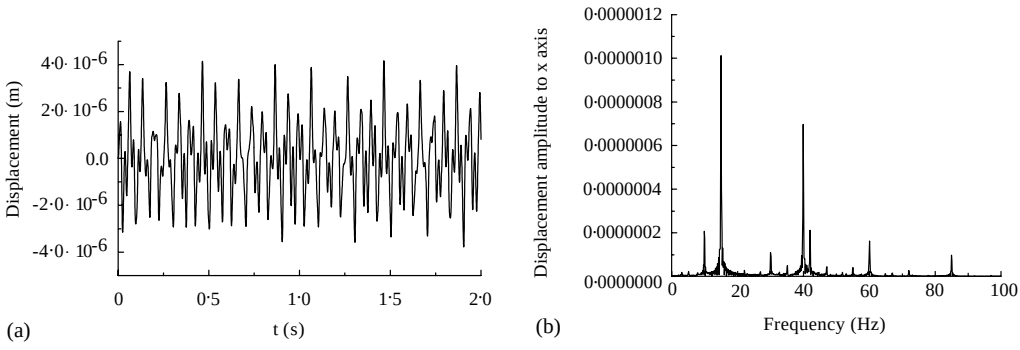

Figure 5. (a) The displacement to time when UMP existing, and $p = 1$, $\Omega = 15$ Hz. (b) Frequency components of the displacement when UMP exists and $p = 1$, $\Omega = 15$ Hz.

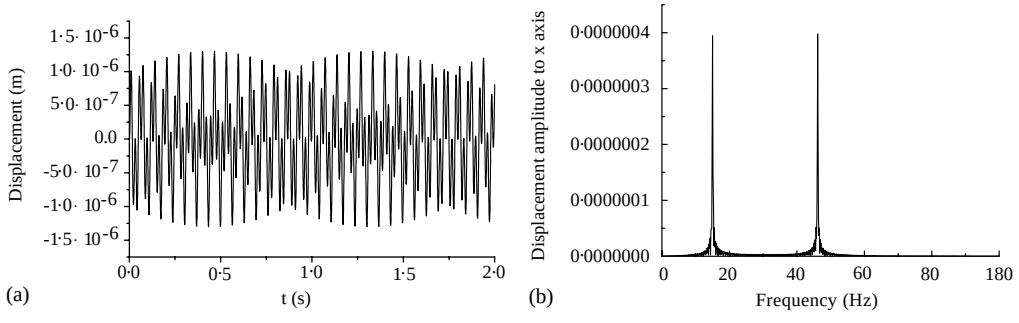

Figure 6. (a) The displacement to time when UMP not existing and $p = 1$, $\Omega = 15$ Hz. (b) Frequency components of the displacement when UMP not existing and $p = 1$, $\Omega = 15$ Hz.

not a pure circle, but a circle with petals. The vibration magnitude is fluctuant due to the UMP. Figure 4(b) shows the curves of the UMP to time. Figure 4(c) shows its frequency components. From Figure 4(c), it can be seen that the UMP includes the component of rotating frequency (5 Hz) and the component of combination of the double-power frequency minus rotating frequency (95 Hz). According to the theory of linear rotor dynamics, when the rotor is whirling stably, we have $\boldsymbol{\theta} = \boldsymbol{\Omega t} + \phi$ in Figure 1, where $\boldsymbol{\phi}$ is the angle difference between the displacement of the rotor center and the eccentricity force. Therefore, from equation (13), we can see that the UMP should include the components of 5, 95, and 85 Hz.The magnitude in the component of 85 Hz is much less than that in 5 and 95 Hz from Figure 4(c).

Figures 5 and 6 show the situation for $\mathbf{p} = 1$ and $\boldsymbol{\Omega} = 15$ Hz. The damping c is not considered here for sake of studying the natural frequency of the system. Figure 5(a) shows the curves of the displacement projecting to x-axis when both the UMP and the eccentric force exist. Figure 5(b) shows its frequency components. Figure 6(a) shows the situation when the UMP does not exist. Figure 6(b) shows its frequency components. From Figures 5 and 6, it can be seen that if the UMP does not exist, the displacement contains the component of rotating speed (15 Hz) and the component of natural frequency (46 Hz), but if the UMP exists, the displacement contains many kinds of frequency components, such as the component of rotating speed (15 Hz), the component of combination of the double-power frequency minus rotating frequency (85 Hz). It can be observed that the peak

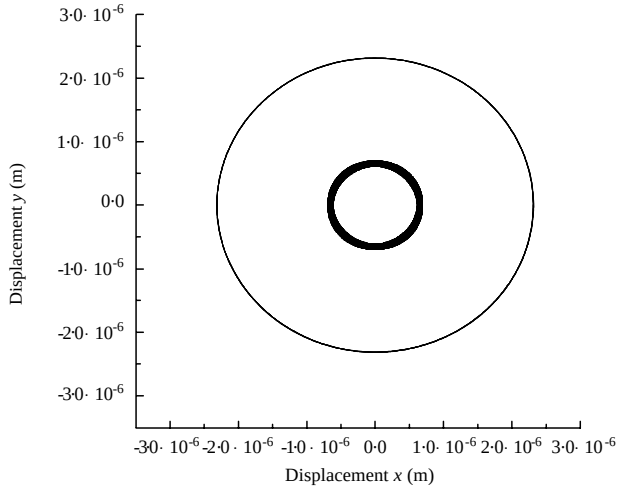

Figure 7. Rotor center orbits when $p = 3$, $\Omega = 15$ Hz.

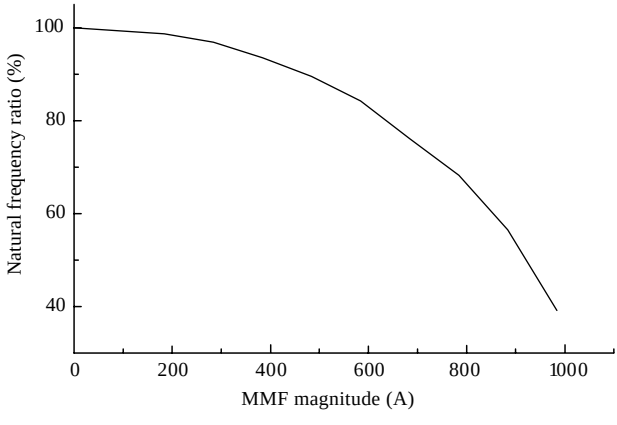

Figure 8. The relation between MMF magnitude and natural frequency ratio.

corresponding to 46 Hz when the UMP does not exist moves to a peak at 40 Hz with a short peak at 43 Hz when the UMP exists. This can be explained from Appendix A. The linear component of the UMP functions as a negative stiffness, which reduces the natural frequency of the system. We have found peaks corresponding to 10, 30, and 60 Hz from Figure 5(b) too. It is not clear how to explain these peaks. When the damping **c** is considered, all other frequency components disappear except the component of rotating speed (15 Hz) and the component of combination of the double-power frequency minus rotating frequency (85 Hz) as shown in Figure 5(b).

Figures 7 and 8 show the results for $\mathbf{p} = 4$. If $\mathbf{p} > 3$, it can be observed that from equation (13), the component of the UMP oscillated with double power frequency disappears, and only the constant unbalanced magnetic pull remains. Figure 7(a) shows the rotor center orbit with UMP existing and not existing when $\mathbf{p} = 4$ and $\boldsymbol{\Omega} = 15$ Hz. Two circular orbits can be observed. Figure 8 shows the relation between the MMF magnitude (which is directly proportional to the rotor excitation current) and the natural frequency ratio ($= 100 \times$ natural frequency with UMP existing/natural frequency with UMP not existing)

when the mean air gap is invariable. It can be observed that when the MMF magnitude increases, the natural frequency ratio reduces, and the curve is non-linear. It means that the more the MMF magnitude increases, the more quickly the natural frequency reduces.

From the above discussion, we can conclude that the UMP increases the vibration magnitude and reduces the natural frequency. When $\mathbf{p} = 1$, the center orbit is a circle with petals. When the relative eccentricity is small, the non-linear characteristics of the vibratory responses are not obvious.

3.2. WHEN THE RELATIVE ECCENTRICITY IS LARGE

From Figure 3, it can be seen that the curves of $\mathbf{f}_1$, $\mathbf{f}_2$, $\mathbf{f}_3$ and $\mathbf{f}_4$ are all non-linear when the relative eccentricity is large. Considering a fact that the rotor axis is positioned parallel to, rather than being on, the stator axis, static eccentricity can occur in this case. An initial static eccentricity $\mathbf{r}_0 = 0{\cdot}001$ m is given to the rotor axis toward the positive axis **x**, while the stator axis is on the origin of the coordinate. Because of the mass eccentricity, dynamic eccentricity also exists together with the static eccentricity in this situation. Figures 9–13

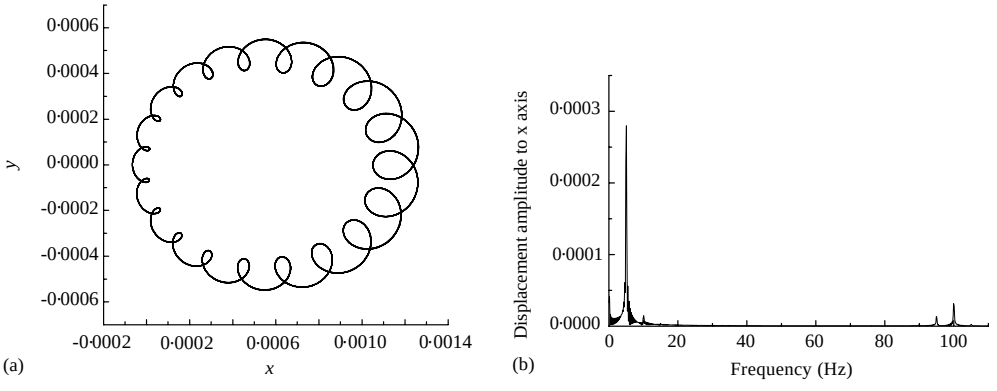

Figure 9. (a) Rotor center orbit when $p = 1$, $\Omega = 5$ Hz and $r = 0{\cdot}001$ m. (b) Frequency components of the displacement when $p = 1$, $\Omega = 5$ Hz and $r = 0{\cdot}001$ m.

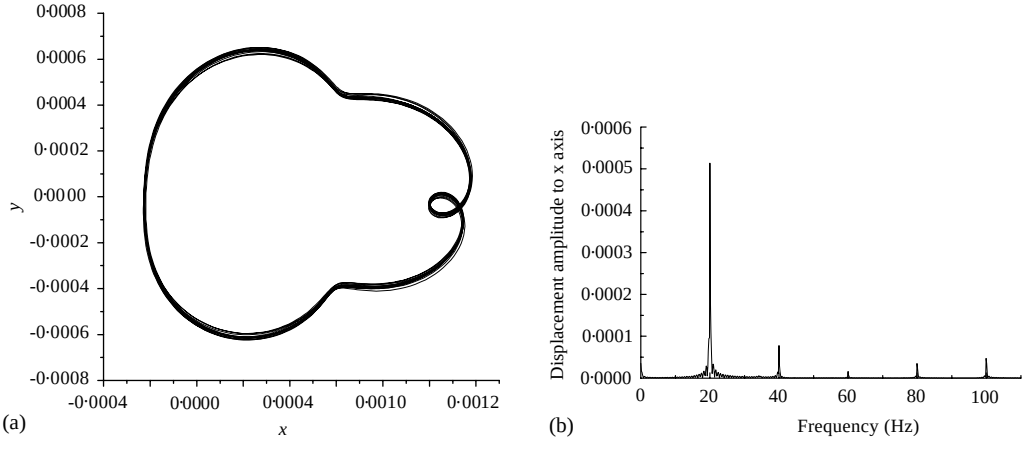

Figure 10. (a) Rotor center orbit when $p = 1$, $\Omega = 20$ Hz and $r = 0{\cdot}001$ m. (b) Frequency components of the displacement when $p = 1$, $\Omega = 20$ Hz and $r = 0{\cdot}001$ m.

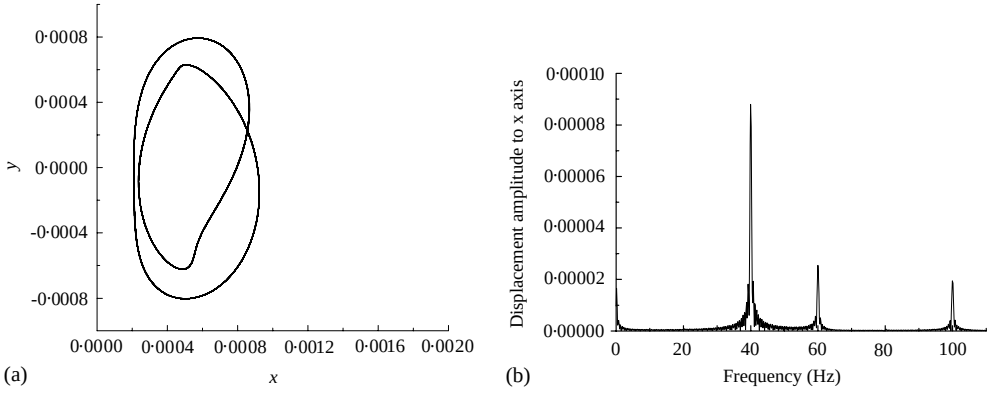

Figure 11. (a) Rotor center orbits when $p = 1$, $\Omega = 40$ Hz and $r = 0{\cdot}001$ m. (b) Frequency components of the displacement when $p = 1$, $\Omega = 40$ Hz and $r = 0{\cdot}001$ m.

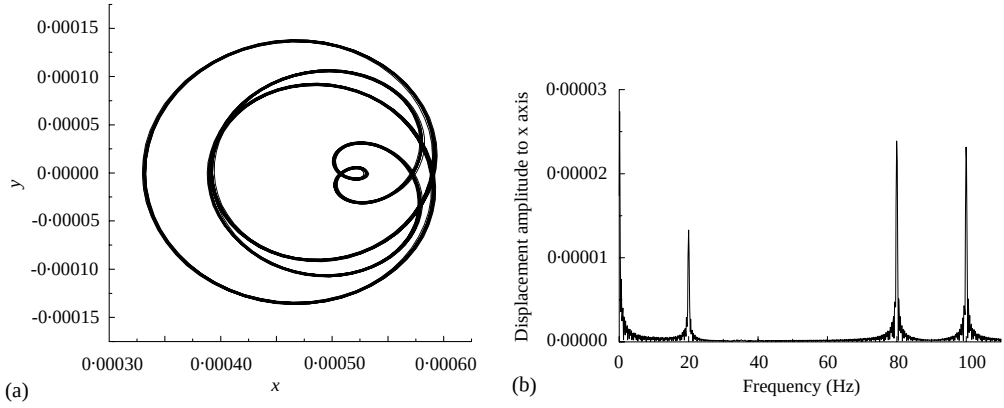

Figure 12. (a) Rotor center orbits when $p = 1$, $\Omega = 80$ Hz and $r = 0{\cdot}001$ m. (b) Frequency components of the displacement when $p = 1$, $\Omega = 80$ Hz and $r = 0{\cdot}001$ m.

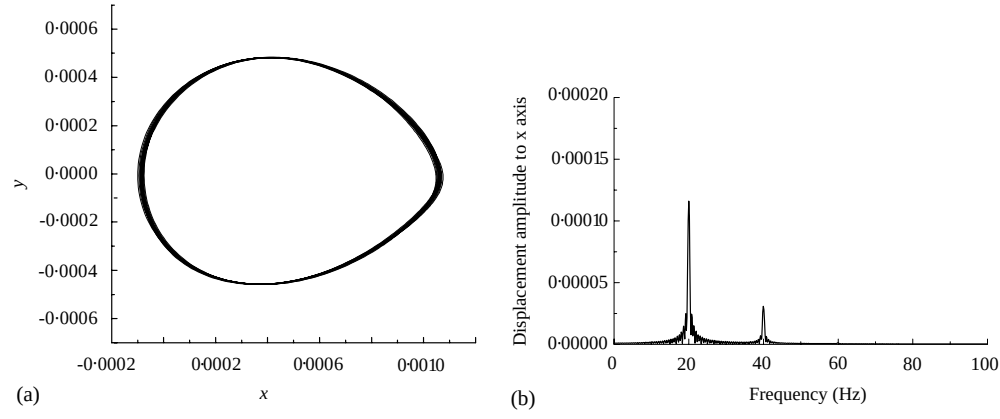

Figure 13. (a) Rotor center orbits when $p = 4$, $\Omega = 20$ Hz and $r = 0{\cdot}001$ m. (b) Frequency components of the displacement when $p = 4$, $\Omega = 20$ Hz and $r = 0{\cdot}001$m.

show many kinds of periodic center orbits and the frequency components of displacements at different rotating speeds when $\mathbf{p} = 1$ or 4. Figure 9 shows the results for ($\mathbf{p} = 1$, $\mathbf{\Omega} = 5$ Hz). Figures 10–13 show the results for ($\mathbf{p} = 1$, $\mathbf{\Omega} = 20$), ($\mathbf{p} = 1$, $\mathbf{\Omega} = 40$), ($\mathbf{p} = 1$, $\mathbf{\Omega} = 80$ Hz) and ($\mathbf{p} = 4$, $\mathbf{\Omega} = 20$ Hz) respectively. From the center orbits in Figures 9–13, it can be seen that the orbits are not axisymmetric due to the non-linear UMP. For different rotating speeds, the center orbits when $\mathbf{p} = 1$, are various. When $\mathbf{\Omega} = 5$ Hz, the center orbit is an ellipse with petals or smaller circles (depending on the value of the eccentric force and the UMP force) round its circumference. In Figure 10(a) for $\mathbf{\Omega} = 20$ Hz, the center orbit is a closed out-of-shape curve, whose periodicity is synchronous to the rotating speed. In Figure 10(a) for $\mathbf{\Omega} = 40$ Hz and Figure 12(a) for $\mathbf{\Omega} = 80$ Hz, the center orbits are closed curves with periodicity being two and four times of the rotating speed respectively. The frequency components of the displacement response are obtained by the harmonic analysis. The results are shown in Figures 9(b)–13(b). It can be seen that if $\mathbf{p} = 1$, the dynamic responses contain the component of the rotating speed, the component of the double-power frequency minus rotating speed, and the component of the double-power frequency. From Figure 10(b), it can be seen that the vibrations with the double and three times of the rotating frequency are excited by the non-linear UMP. From Figure 13(b), vibrations with the double rotating frequency are excited as well.

4. CONCLUSIONS

The method based on the idea of modulating the fundamental MMF wave by air-gap permeance expressed as a Fourier series is used in this paper. The analytical expression of the UMP in a three-phase electric machine with any pole-pairs caused by static eccentricity and dynamic eccentricity is derived. The non-linear vibratory responses of a Jeffcott rotor excited by the UMP and the eccentric force are studied by use of the numerical method —the Newmark method. From the results, it can be concluded that:

(1) The UMP includes the constant component and oscillatory components. The frequency of the oscillatory component is the double-supply frequency. If the pole-pair number is larger than three, only the constant unbalanced magnetic pull remains. When the eccentricity is large, the magnitude of the UMP is non-linear.
(2) Due to the UMP, the natural frequency of the rotor system will be reduced and the magnitude of vibration will become larger. The orbits of the rotor center are axisymmetry, when the relative eccentricity is small.
(3) When the relative eccentricity is large, the center orbits are not axisymmetry due to the non-linear UMP. If $\mathbf{p} = 1$, the dynamic response contains the component of rotating speed, the component of the double power frequency minus rotating speed, and the component of the double power frequency.
(4) Vibrations with double and three times of the rotating frequency can be excited by the non-linear UMP.

ACKNOWLEDGMENTS

This research is supported by National Natural Science Foundation of China (Grant No. 19990510) and Tsinghua University Basic Research Foundation (Grant No. Jc1999045).

REFERENCES

1. P. VON KAEHNE 1963 *Report Ref. Z/T*-142, *Electrical Research Association*, *U.K.* Unbalanced magnetic pull in rotating electrical machines. Survey of published work.
2. K. J. BINNS and M. DYE 1973 *Proceedings of the IEE* **120**, 349–354. Identification of principal factors causing unbalanced magnetic pull in cage induction motors.
3. E. W. SUMMERS 1955 *Transactions of the American IEE* **74**, 69–72. Vibration in 2-pole induction motors related to slip frequency.
4. J. FRUCHTENICHT, H. JORDAN and H. O SEINSCH 1982 *Archives of Elektrotech* **65**, 271–292. Running instability of cage induction motors caused by harmonic fields due to eccentricity. Part 1. Electromagnetic spring constant and electromagnetic damping coefficient. Part 2. Self-excited transverse vibration of the rotor.
5. R. BELMANS, W. GEYSEN, H. JORDAN and A. VANDENPUT 1982 *Proceedings*, *International Conference on Electrical Machines-Design and Application*, *London*, 916–921. Unbalanced magnetic pull and homopolar flux in three-phase induction motor with eccentric rotors.
6. R. BELMANS, W. GEYSEN, H. JORDAN and A. VANDENPUT 1982 *Proceedings*, *International Conference on Electrical Machines-Design and Application*, *London*, 65–69. Unbalanced magnetic pull in three-phase two-pole motors with eccentric rotor.
7. A. C. SMITH and D. G. DORRELL 1996 *IEE Proceedings of the Electrical Power Applications* **143**, 193–201. Calculation and measurement of unbalanced magnetic pull in cage induction motors with eccentric rotor. Part 1. Analytical modal.
8. S. SALON, M. DEBORTOLA, D. BURROW and C. SLAVIK 1992 *Proceedings*, *International Conference on Electrical Machines-Design and Application*, *London*, 371–375. Calculation of circulating current between parallel windings in induction motors with eccentric rotor by the finite element method.
9. M. J. DEBORTOLA, S. J. SALON, D. W. BURROW and C. J. SLAVIK 1993 *IEEE Transactions on Magnetics* **29**, 1676–1682. Effect of rotor eccentricity and parallel windings on induction machine behaviour: a study using finite element analysis.
10. R. BELMANS, A. VANDENPUT and W. GEYSEN 1987 *Proceedings of the IEE Part B* **134**, 101–109. Influence of unbalanced magnet pull on the radial stability of flexible-shaft induction machines.
11. Z. Q. ZHU and D. HOWE 1997 *Electric Machine and Power Systems* **25**, 443–457. Effect of Rotor eccentricity and magnetic circuit saturation on acoustic noise and vibration of single-phase induction motors.
12. H. JORDAN, R. D. SCHRÖDER and H. O. SEINSCH 1981 *Archives of Elektrotech* **63**, 117–124. Zur Berechnung einseitig magnetischer Zugkräfte in Drehfeld-Maschinen.
13. S. J. CHAPMAN 1999 *Electric Machinery Fundamentals*. Boston: McGraw-Hill.
14. D. G. DORRELL 1999 *IEEE Transactions on Energy Conversion* **14**, 304–309. Experimental behaviour of unbalanced magnetic pull in 3-phase induction motors with eccentric rotors and the relationship with tooth saturation.
15. N. NEWMARK 1959 *Journal of Engineering and Mechanical Division of American Society of Civil Engineers* **85**, 67–94. A method of computation for structural dynamics.

APPENDIX A

Equation 13(a) and (b) can be written as

$$P^{UMP} = P_x^{UMP} + \mathrm{i}P_y^{UMP} = \begin{cases} f_1 \mathrm{e}^{\mathrm{i}\theta} + f_2 \mathrm{e}^{\mathrm{i}(2\omega t - \theta)} + f_3 \mathrm{e}^{-\mathrm{i}(2\omega t - 3\theta)}, & p = 1, \\ f_1 \mathrm{e}^{\mathrm{i}\theta} + f_3 \mathrm{e}^{\mathrm{i}(2\omega t - 3\theta)} + f_4 \mathrm{e}^{-\mathrm{i}(2\omega t - 5\theta)}, & p = 2, \\ f_1 \mathrm{e}^{\mathrm{i}\theta} + f_4 \mathrm{e}^{\mathrm{i}(2\omega t - 5\theta)}, & p = 3, \\ f_1 \mathrm{e}^{\mathrm{i}\theta} & p > 3. \end{cases} \tag{A.1}$$

From equation (A.1), it can be obtained that $\mathbf{f}_1$ is the amplitude of the constant UMP, $\boldsymbol{\theta}$ is its direction angle. From Figure 1, we can obtain that the constant UMP always points to the minimum air gap. $f_1 \mathrm{e}^{\mathrm{i}\theta}$ is the mean value of the UMP and others are the oscillating components.

Substituting equation (4) into equation (14) gives

$$f_1 = \frac{RL\pi\mu_0 F_j^2}{\delta_0^2}\frac{1}{1-\varepsilon^2}\left[\frac{1-\sqrt{1-\varepsilon^2}}{\varepsilon} + \left(\frac{1-\sqrt{1-\varepsilon^2}}{\varepsilon}\right)^3 + \left(\frac{1-\sqrt{1-\varepsilon^2}}{\varepsilon}\right)^5\right], \quad \text{(A.2a)}$$

$$f_2 = \frac{RL\pi\mu_0 F_j^2}{2\delta_0^2}\frac{1}{1-\varepsilon^2}\left[\frac{1-\sqrt{1-\varepsilon^2}}{\varepsilon} + \left(\frac{1-\sqrt{1-\varepsilon^2}}{\varepsilon}\right)^3 + \left(\frac{1-\sqrt{1-\varepsilon^2}}{\varepsilon}\right)^5\right], \quad \text{(A.2b)}$$

$$f_3 = \frac{RL\pi\mu_0 F_j^2}{4\delta_0^2}\frac{1}{1-\varepsilon^2}\left(\frac{1-\sqrt{1-\varepsilon^2}}{\varepsilon}\right)^3, \quad \text{(A.2c)}$$

$$f_4 = \frac{RL\pi\mu_0 F_j^2}{2\delta_0^2}\frac{1}{1-\varepsilon^2}\left(\frac{1-\sqrt{1-\varepsilon^2}}{\varepsilon}\right)^5. \quad \text{(A.2d)}$$

Because $[\varepsilon^2] < 1$, we can obtain the following expression of the power series by keeping the first two terms:

$$\frac{1}{1-\varepsilon^2} \approx 1 + \varepsilon^2, \qquad \sqrt{1-\varepsilon^2} \approx 1 - \frac{1}{2}\varepsilon^2. \quad \text{(A.3)}$$

Substituting equation (A.3) into equation (A.2) and neglecting terms with power number being greater than three give

$$f_1 \approx \frac{RL\pi\mu_0 F_j^2}{\delta_0^2}\left(\frac{1}{2}\varepsilon + \frac{5}{8}\varepsilon^3\right), \quad \text{(A.4a)}$$

$$f_2 \approx \frac{RL\pi\mu_0 F_j^2}{\delta_0^2}\left(\frac{1}{4}\varepsilon + \frac{5}{16}\varepsilon^3\right), \quad \text{(A.4b)}$$

$$f_3 \approx \frac{RL\pi\mu_0 F_j^2}{8\delta_0^2}\varepsilon^3, \quad \text{(A.4c)}$$

$$f_4 \approx O(\varepsilon^5). \quad \text{(A.4d)}$$

From equations (3) and (A.4a), we have

$$f_1 e^{i\theta} = \frac{RL\pi\mu_0 F_j^2}{2\delta_0^3}(x + iy) + \frac{5RL\pi\mu_0 F_j^2}{8\delta_0^2}\varepsilon^3 e^{i\theta}. \quad \text{(A.5)}$$

First component on the right side of equation (A.5) is linear in x and y and it provides a negative stiffness which reduces the natural frequency of the system.

APPENDIX B: NOMENCLATURE

(x, y)	co-ordinates of the rotor center
r	distance from stator center to rotor center
$\mathbf{r}_0$	initial static eccentricity

$\boldsymbol{\delta}$	air-gap length
$\boldsymbol{\delta}_0$	mean air-gap length
$\boldsymbol{\varepsilon}$	relative eccentricity
$\boldsymbol{\mu}_0$	air permeance
$\mathbf{F}$	fundamental MMF of the air gap
$\mathbf{F}_j$	fundamental MMF amplitude of the rotor exciting current
$\boldsymbol{\sigma}$	stress normal to the rotor boundary
$\mathbf{t}$	time
Δt	time step
$\boldsymbol{\beta}$, $\boldsymbol{\gamma}$	Newmark integral parameters
$\boldsymbol{\lambda}$	accuracy error
$\boldsymbol{\omega}$	the supply frequency
$\mathbf{p}$	pole-pair number of the generator
$\mathbf{B}$	air-gap flux density
$\mathbf{k}$	spring coefficient of the rotor
$\mathbf{c}$	damping coefficient of the rotor
$\mathbf{m}$	rotor mass
$\mathbf{a}$	mass eccentric distance
$\boldsymbol{\Omega}$	rotating angular speed
$\mathbf{R}$	radius of the generator rotor
$\mathbf{L}$	length of the generator rotor
α, θ, ϕ	angles
Λ	air-gap permeance
Λ_n	Fourier coefficients of Λ
$\bar{\Lambda}_n$	normalized permeance series magnitude
P^{UMP}, P_x^{UMP}, P_y^{UMP}	values of the UMP force and components projecting to axis x and y
P^e	vector of the mass eccentric force
f_1, f_2, f_3, f_4	amplitudes of components of the UMP
ω_n	natural frequency of the system